AN AUTOMATICALLY APPROACH OF SPACE OBJECTS DETECTION

Cristian Omat(1,2), Mirel Birlan(1,2,3), Dan Alin Nedelcu(2)

(1) University of Bucharest, Doctoral School of Physics, 405 Atomistilor street, Magurele, Romania, Email: doctorat@fizica.unibuc.ro
(2) Astronomical Institute of the Romanian Academy, 5 Cutitul de Argint, Bucharest, Romania, Email: astro@astro.ro
(3) Laboratoire Temps-Espace, Observatoire de Paris, 77 Avenue Denfert-Rochereau, 75014 Paris Cedex, France, Email: scar.imcce@obspm.fr

ABSTRACT

A highly effective approach to satellite and space debris monitoring involves advanced machine learning (ML) techniques. This study introduces an ML-driven solution for object detection and classification, employing the You Only Look Once (YOLO) algorithm, a convolutional neural network (CNN) based model that excels in real-time object recognition. YOLO's single-pass prediction capability enables rapid and accurate detection, essential for applications with large-scale data acquisition. During this project, 1,411 images from an all-sky camera [1] installed at Berthelot Observatory (IAU Code L54) were processed to detect the space objects (active satellites and debris) during several observational campaigns. Following the training, tunning and validation steps, the performance of our model leads 95.5% accuracy and 91% precision.

1 INTRODUCTION

The unprecedented surge in satellite deployment projects numbers up to 100,000 new launches by the end of 2030 [2] and [3]. A substantial number of these satellites is expected to be concentrated in Low Earth Orbit (LEO) regions, altitudes of up to 2,000 km, favored for their operational advantages, such as reduced deployment costs and minimal communication latency. Given the magnitude of this expansion, there is a critical need for enhanced automation in the monitoring of space objects.

The convolutional neural network (CNN) architecture allows for efficient feature extraction through convolutional layers, generating bounding boxes around detected objects. One of these CNN approaches which also generates bounding boxes around detected objects is You Only Look Once (YOLO) algorithm. It's operational efficiency, superior to many conventional detection methods, stems from the ability to analyse entire images in a single pass, a quality that significantly enhances processing speed [4].

Deployed in February 2025, YOLO12 is the newest version of YOLO Algorithm, a computer vision model architecture developed by Ultralytics [4]. The latest iteration of YOLO, presented by Ultralytics as "YOLO12: Attention-Centric Object Detection", adopts a distinct approach that diverges from the traditional CNN-based solutions integrated in earlier versions. The developers assert that this model achieves substantial improvements in accuracy compared to its predecessors, with some compromises in terms of speed, a phenomenon that we also observed during our training process.

According to the Ultralytics press release (February 20, 2025), the main advantages of YOLO12 are the new Area Attention Mechanism, Residual Efficient Layer Aggregation Networks (R-ELAN), the optimized attention architecture, the comprehensive task support, the enhanced efficiency and the flexible deployment [4].

The goal of this study was to evaluate the new detection algorithm using a minimal dataset of FITS images acquired from an all-sky camera. For this purpose, we used the Python package option developed by Ultralytics. The results were promising and in the next phase, we will rectify the issues encountered and subsequently move on to the space object classification stage.

The paper is organized as following: in the section 2 the process of data acquisition is presented followed by the methodology (section 3) and the results (section 4). Finally, the conclusions are presented in the section 5.

2 DATA PREPARATION

The dataset consists of all-sky images coming from the Meteorites Orbits Reconstruction by Optical Imaging (MOROI) infrastructure [1] and [5]. This is a sky-surveillance camera network operated by Astronomical Institute of the Romanian Academy (AIRA).

For this study we used an all-sky camera located at Berthelot Observatory (IAU Code L54) based on the 4.9 x 3.6 mm Sony CCD chip ICX445 (1296 x 966 active pixels, 12 bit dynamic range), resulting in a 3.75 x 3.75 µm pixel size. [5]

Proc. 9th European Conference on Space Debris, Bonn, Germany, 1–4 April 2025, published by the ESA Space Debris Office
Editors: S. Lemmens, T. Flohrer & F. Schmitz, (http://conference.sdo.esoc.esa.int, April 2025)

During of nine observational sessions conducted between January and February 2025, a dataset comprising 1,589 images in FITS format was extracted from 96 known space objects observable transits. For each pass, the all-sky system was scheduled to continuously acquire images with 3 or 5 seconds exposure time.

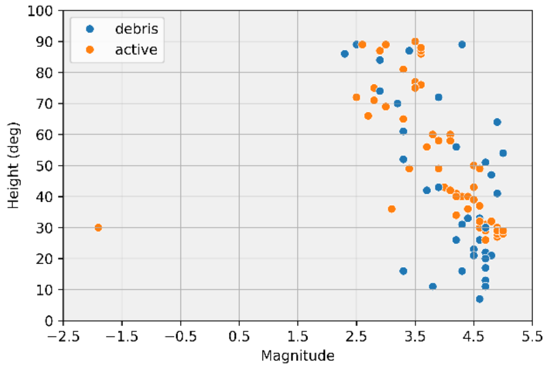

Figure 1. Data Overview: active satellites and debris

These objects were subsequently classified into two primary categories: active satellites and space debris (rocket bodies and inactive satellites), based on information from the literature [6]. *Figure 1* reveal a clustering of space objects within the higher magnitude interval (between +3.5 and +5) in the area of 20 – 45 degrees above the horizon. Further analysis of our dataset indicates that active satellites are primarily composed of those belonging to the Starlink mega-constellation. Moreover, we have identified a transit by the International Space Station (ISS). In the *Figure 2,* it can be observed that most of the recorded objects were from Low Earth Orbit (LEO), characterized by orbits with very low eccentricities, almost circular. However, the dataset also includes five debris objects (Centaur D-1A AC-31, Breeze M-DEB, Breeze M-DEB (Tank), CZ-3A RB and Cosmos 2344) from Medium Earth Orbit (MEO), which were detectable due to their high orbital eccentricities and, consequently, of their low perigee values.

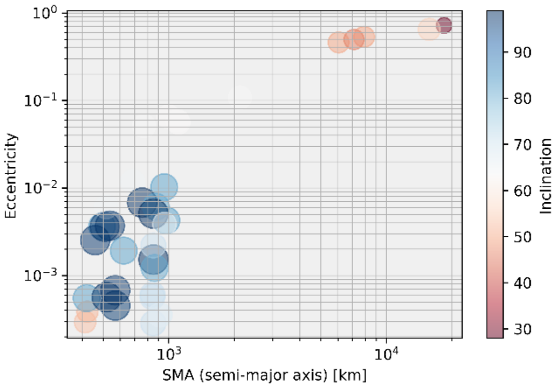

Figure 2. Correlation of orbital parameters

Following the analysis of the dataset, it can be observed in the *Figure 3* that the detection limit of the setup used for the observational campaigns extends up to 6,000 km, e.g Centaur D-1A AC-31 and CZ-3A RB.

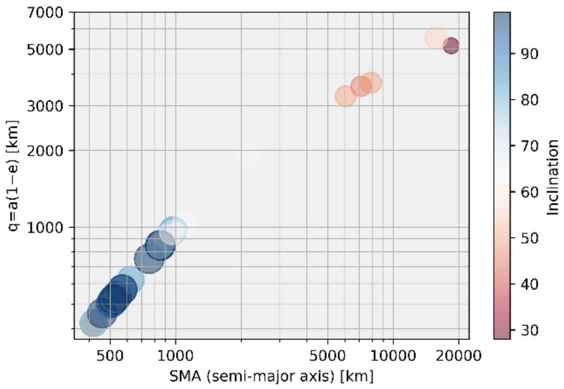

Figure 3. Detection limit

3 METHODOLOGY

The planning of observations was designed to record the space objects at their point of maximum altitude on celestial sphere, as in [7]. We extracted the ephemeris for Berthelot Observatory (IAU Code L54) from the online database [6] over several weeks of observation, covering both morning and evening periods. For the calibration of the data acquiring workflow, we initially chose to record brighter objects (magnitude limit +3). After the analysis of the initial dataset, we decided to modify the magnitude limit to +5, to detect even more space objects. Furthermore, during the first observation night, we tested a exposure duration of 3 seconds for each frame. This exposure time shows that the trails (satellites and debris) on the images were not sufficiently distinct. Consequently, we changed the strategy of observations for an exposure time of 5 seconds.

We decided to acquire a total of 40 images (5s/ exposure) for each object in the list—20 captured prior to the moment of maximum high and 20 captured afterward. On a daily basis, we reviewed the recorded data sets to validate the images suitable for progression to the next stage: constructing a consistent dataset for machine learning (ML) training. In the end, 1,589 valid images were included in this set. From these, 1,411 images were selected and subsequently divided based on their intended purpose. This was done using the open-source online computer vision platform Roboflow, as follows: 988 images (70%) for the training set, 282 images (20%) for the validation set, and 141 images (10%) for the test set [8]. In the subsequent step, we manually annotated the trails in the images by employing bounding boxes to delineate the areas of interest. Finally, we exported the dataset in YOLO12 format for training step in Python using the Ultralytics library [4].

4 RESULTS

The trails detection model was trained for 50 epochs, batch size of 16 and the process was completed in 0.429 hours. The performance was evaluated using mean average precision (mAP50) at 94,1%. This threshold is often chosen as it provides a balance between precision and recall, allowing model evaluation based on detecting objects with a minimum 50% overlap.

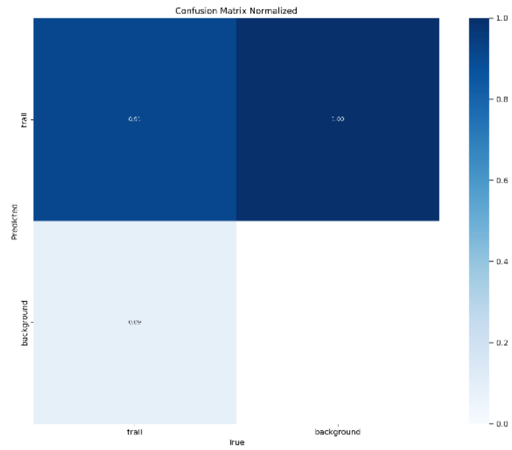

Figure 4. Confusion matrix normalized

In the Confusion Matrix *(Figure 4)* it can be observed the results of the model: TP (True Positive) = 0.91; TN (True Negative) = 1; FP (False Positive) = 0.09 and FN (False Negative) = 0. Based on these values, the following performance parameters can be calculated:

$$Accuracy = \frac{TP + TN}{\mathrm{TP + TN + FP + FN}} = 0.955 \qquad (1)$$

The model demonstrates a high level of accuracy, indicating that it correctly classifies the majority of instances, achieving an accuracy rate of 95,5%.

$$Precision = \frac{TP}{\mathrm{TP + FP}} = \ 0.91 \qquad (2)$$

The precision of the model is relatively good, indicating that when the model predicts “trail”, it is correct 91% of the time. There is a low risk of incorrectly classifying “background” as 'trail.

$$Recall = \frac{TP}{\mathrm{TP + FN}} = 1 \qquad (3)$$

The recall of the model is perfect, indicating that it correctly identifies all instances of “trail”. There are no “trails” that the model fails to detect.

$$F1\ Score = \frac{2\ x\ Precision\ x\ Recall}{Precision + \ Recall} = \ 0.953 \qquad (4)$$

The F1-score indicate a strong balance between precision and recall, suggesting that the model exhibits good overall performance.

$$Specificity = \frac{\mathrm{TN}}{\mathrm{TN + FP}} = \ 0.917 \qquad (5)$$

The specificity of the model is quite good, indicating that it correctly identifies the majority of instances of “background” (91.7%). There is a low risk of incorrectly classifying “trail” as “background”.

Based on these results, we can affirm that the model exhibits excellent performance and it demonstrates high accuracy and a strong balance between precision and recall. Furthermore, perfect recall suggests that the model is highly effective at identifying all instances of “trail”.

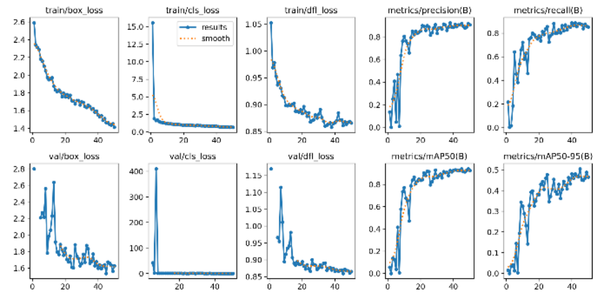

Figure 5. Loss and Metrics for the detection model

The graphs presented in *Figure 5* are used to monitor and analyse the performance of a machine learning model during the training and validation processes, being essential tools for diagnosing and improving machine learning models. Analysis of the loss graphs during the training (train) and validation (val) stages for box_loss, cls_loss, and dfl_loss reveals a general downward trend over the epochs, indicating that the model is learning and improving. However, it should be noted that the validation graphs reveal greater fluctuations compared to the training graphs. The significant fluctuations observed in the validation graphs may suggest a slight overfitting, particularly towards the end of the training process.

The metrics graphs for precision, recall, mAP50, and mAP50-95 demonstrate a general upward trend throughout the training process. This indicates that the model is becoming increasingly accurate and effective at identifying and localizing objects.

To demonstrate the effectiveness of our trail detection model, we extracted a random sample from the prediction folder. As shown in *Figure 6*, we observed two types of detections within the same image: either one trail or multiple trails. Additionally, there were samples where the "background" was detected, indicating no trail present, as illustrated in *Image 72* of the *Figure 6*. In the *Image 68* of the *Figure 6*, two trails were detected with confidence scores of 82% and 75%, showcasing a clear example of the model's effectiveness.

In our final analysis, we examined all 141 images from the test set and found that 101 images contained a single detection, while 32 images had multiple detections. Furthermore, 8 images were predicted as "background," indicating no trail present. These results underscore the model's capability in accurately identifying and localizing trails within various contexts.

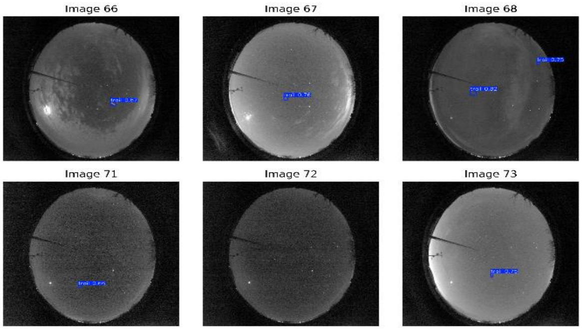

Figure 6. Confidence scores for a random samples set: Image 66 (0.87), Image 67 (0.76), Image 68 (0.82, 0.75), Image 71 (0.66), Image 72 - no trail, Image 73 (0.75)

5 CONCLUSIONS

Based on the analysis of the confusion matrix, loss curves, and performance metrics, we can conclude that our detection model has been trained effectively, though opportunities for further optimization remain. It should be mentioned that our test model was trained on a small sample of images and most of the space objects were relatively fainter (magnitude between +3.5 and +5).

As strengths, we can highlight the overall good accuracy of 95.5%, excellent background detection, and relatively strong performance metrics, indicating decent model effectiveness. It is observed that there are instances where the model confuses “trail” with “background”. However, these situations are relatively rare, accounting for only 9% of cases. Our study further revealed that filtering false detections is crucial for enhancing accuracy, particularly through multiple confidence threshold values and employing Non-Maximum Suppression (NMS), which retains just the best detection. Overall, the model is well-trained and operates within optimal parameters, but the it can be improved for “trail” detection.

As a result of this test, which represents the initial phase of a larger project, several issues have been identified that need to be addressed before proceeding to the next step, namely classification. A solution is to increase the training dataset, because this test iteration was performed on a modest sample of images. Also, we plan to implement several data augmentation techniques [8], which would also reduce overfitting. Furthermore, issues related to image quality have been identified, necessitating the automation of the all-sky camera calibration procedure for the collection of bias, flat, and dark frames. New tests are required to improve overall detection accuracy and performance.

6 REFERENCES

1. Nedelcu, A. D., Birlan, M., Turcu, V., Badescu, O., Boaca, I., Gornea, A., Blagoi, O., Danescu, C., Paraschiv, P. (2018) . The MOROI network. Meteorites Orbits Reconstruction by Optical Imaging, *Outlook in Astronomy, Astrophysics, Space and Planetary Sciences,* p. 21.

2. Boley, A. C., Byers, M. (2021). Satellite mega-constellations create risks in low earth orbit, the atmosphere and on earth., *Scientific Reports* 11(1).

3. Williams, A., Hainaut, O., Otarola, A., Tan, G.H., Rotola, G. (2021). Analysing the impact of satellite constellations and ESO’s role in supporting the astronomy community., *arXiv:*2108.04005.

4. Tian, Y., Ye, Q., Doermann, D. (2025). YOLOv12: Attention-Centric Real-Time Object Detectors, arXiv preprint arXiv:2502.12524

5. Anghel, S., Nedelcu, D. A., Birlan, M., Boaca, I. (2023). Single-station meteor detection filtering using machine learning on MOROI data. *Monthly Notices of the Royal Astronomical Society*, 518(2), 2810-2824.

6. Peat, C. (2025). Heavens-Above. *http://www.heavens-above.com*.

7. Halferty, G., Reddy, V., Campbell, T., Battle, A., Furfaro, R. (2022). Photometric characterization and trajectory accuracy of Starlink satellites: implications for ground-based astronomical surveys. *Monthly Notices of the Royal Astronomical Society*, 516(1):1502–1508.

8. Dwyer, B., Nelson, J., Hansen, T., et. al. (2024). Roboflow (Version 1.0) [Software]. *Available from https://roboflow.com.*